NUCLEAR SCIENCE AND ENGINEERING: **175**, 172–187 (2013)

Development of an Adaptive Nonintrusive Spectral Technique for Uncertainty Quantification and Application to a Multiphysics Problem

L. Gilli,* D. Lathouwers, J. L. Kloosterman, and T. H. J. J. van der Hagen

Delft University of Technology, Delft, The Netherlands

Received October 8, 2012
Accepted January 31, 2013

Abstract—*In this paper we present the derivation and the application of an adaptive nonintrusive spectral technique for uncertainty quantification. Spectral techniques can be used to reconstruct stochastic quantities of interest by means of a Fourier-like expansion. Their application to uncertainty propagation problems can be performed in a nonintrusive fashion by evaluating a set of projection integrals that is used to reconstruct the spectral expansion. We present the derivation of a new adaptive quadrature algorithm, based on the definition of a sparse grid, which can be used to evaluate these spectral coefficients. This new adaptive algorithm is applied to a reference uncertainty quantification problem consisting of a coupled time-dependent model. The benefits of using such an adaptive method are analyzed and discussed from the uncertainty propagation and computational points of view.*

I. INTRODUCTION

The role of uncertainty analysis in nuclear reactor simulations is becoming increasingly important and challenging as the physical realism of the simulations is constantly increasing. There are different kinds of uncertainties to deal with, some of which are represented by approximations introduced by the model or by the numerical scheme used to solve it; however, one of the most important challenges in uncertainty analysis is to handle the uncertainty present in the input data of the problem (like the material properties or the geometric description of a system). This corresponds to estimating how the lack of knowledge in the input data set influences the simulation outputs used in design and safety analysis. Many techniques have been implemented and used in the field so far, the main methods being statistical and deterministic. The main distinction between the two is that statistical methods are in principle exact and require a large computational effort while deterministic methods rely on model approximations, which make the technique faster compared to the first approach. A common way to propagate uncertainties using a deterministic approach is the application of first-order perturbation techniques based on adjoint formulations. The computational effort required to perform this propagation is relatively small, and the accuracy in the prediction of the output uncertainty for small perturbations is good even for nonlinear problems.[1]

In this paper we present the derivation of a deterministic spectral approach, based on the polynomial chaos expansion (PCE) introduced by Ref. 2. PCE-based techniques were first proposed in Ref. 3 and have been applied so far to different scientific fields, ranging from computational fluid dynamics[4,5] to structural mechanics.[6] They can be categorized into two main branches, intrusive and nonintrusive, according to whether their application involves any mathematical modification of the model for which the uncertainty propagation needs to be performed.

Within the reactor physics field, the application of an intrusive PCE approach was first presented for a neutron diffusion problem by Ref. 7 and later applied to the transport equation in two studies[8,9] for fixed-source and eigenvalue problems. This concept has been extended to spatially random problems and to nonintrusive methods

*E-mail: lucagilli.p@gmail.com

by Ref. 10 while Ref. 11 presents the application of a PCE-based regression technique to a coupled steady-state problem. Regarding time-dependent problems an application in the nuclear field was proposed by Ref. 12 where an intrusive stochastic method is applied to a radionuclide dispersion model. In a recent work,[13] we presented an overview of intrusive and nonintrusive methods when applied to simplified time-dependent problems.

In the present work we present the development of a spectral method that is based on the definition of an adaptive sparse-grid algorithm. This algorithm can be used to apply spectral methods in a nonintrusive fashion, by collecting a set of realizations of the outputs of interest. We also present an illustrative application of the method to a coupled problem that models the time-dependent behavior of a sodium fast reactor.

The paper is structured as follows. First, the main concepts behind the definition of spectral techniques are introduced. Then, the algorithm used to adaptively apply the nonintrusive spectral method is defined. This method is finally used to perform uncertainty analysis of a reference time-dependent problem. Its characteristics and advantages are discussed from the uncertainty propagation and computational points of view.

II. SPECTRAL UNCERTAINTY QUANTIFICATION USING NONINTRUSIVE POLYNOMIAL CHAOS TECHNIQUES

Spectral techniques are based on the representation of stochastic processes by means of a spectral expansion in random space. This spectral representation can be used to reproduce any of the processes involved in a mathematical model defining a physical problem of interest. There are many ways to implement this expansion depending on the type of basis used; one of the most known is the generalized PCE defined using multidimensional orthogonal polynomials. The basis for this spectral representation was first introduced by Ref. 2 (as the homogeneous chaos) in order to reproduce Gaussian processes in a spectral fashion. Reference 14 successively presented a family of orthogonal polynomials, known as the Wiener-Askey scheme, that can be used to extend the theory to different families of stochastic processes.

The first step to implement the spectral expansion from a mathematical point of view is the introduction of a group of independent random variables $\boldsymbol{\xi} = [\xi_1(\theta), \ldots, \xi_N(\theta)]$ (where θ is the domain of the stochastic problem) that can be used as a support for the construction of the basis. The size of this variable set, N, is defined as the minimum number of independent random variables needed to describe the random input data set of the problem, which corresponds in most of the cases to the number of random input parameters. The distribution of these random variables is arbitrary, and in principle one should choose it in order to have an optimal representation of the input data set.

Assuming that these variables have been defined, it is possible, according to the polynomial chaos theory, to approximate any stochastic quantity with a finite standard deviation using a truncated expansion. For example, a generic stochastic quantity $\mathrm{R}(\theta)$ (we do not introduce any constraint whether it belongs to the inputs or the outputs of a mathematical model) can be expanded as

$$\mathrm{R}(\theta) = \sum_{i=0}^{P} r_i \Psi_i(\boldsymbol{\xi}(\boldsymbol{\theta})) \ , \tag{1}$$

where a set of multidimensional polynomials Ψ_i (which are functionals since they depend on $\boldsymbol{\xi}$) belonging to the Wiener-Askey scheme is used and where $P + 1$ is the number of terms in the expansion. This number depends on the highest polynomial degree used by the spectral expansion. If we define the maximum polynomial order as p, the number of terms present in the spectral representation is[15]

$$P + 1 = \frac{(N + p)!}{N!p!} \ .$$

It must be stressed that the maximum polynomial order p is the only approximation introduced by the spectral expansion; in fact, choosing a hypothetical infinite order would generate an infinite expansion representing exactly any stochastic process of interest. The most important characteristic for a polynomial basis Ψ_i to be usable in spectral techniques is its orthogonality property with respect to the following definition of the inner product:

$$\langle \Psi_n, \Psi_m \rangle = \int_{\boldsymbol{\Theta}} \Psi_m(\boldsymbol{\xi}) \Psi_n(\boldsymbol{\xi}) w(\boldsymbol{\xi}) \, d\boldsymbol{\xi} = h_n^2 \delta_{mn} \ ,$$

where w is a weight function (measure), which depends on the polynomial expansion used, and $\boldsymbol{\Theta}$ is the support of the stochastic domain. In Ref. 14, it has been shown that some of the polynomials belonging to the Wiener-Askey scheme are more suitable than others when representing particular random distributions: Hermite polynomials, for example, are the best way to represent Gaussian random variables while Legendre polynomials are most suited for uniform distributions. This implies that, if the proper polynomial basis is chosen, the representation of the random input data of the problem can be obtained by using the least number of terms in the spectral expansion.

When dealing with multidimensional random problems, this orthogonal basis is constructed by a direct tensorization of one-dimensional polynomials. After introducing the multi-index $\boldsymbol{\gamma} = (\gamma_1, \ldots, \gamma_N)$, it is possible to define the set

$$\lambda(k) = \left\{ \boldsymbol{\gamma} : \sum_{i=1}^{N} \gamma_i = k \right\} \ , \tag{2}$$

which can be used to define the k'th-order polynomial expansion as

$$\Gamma_k = \left\{ \bigcup_{\boldsymbol{\gamma} \in \lambda(k)} \prod_{\gamma_1}^{\gamma_N} \psi_{\gamma_i}(\xi_i) \right\} \ .$$

Once the PCE is defined, it is possible to represent any of the stochastic quantities involved in the problem (for example, unknowns and responses) by using the same spectral representation. Applying spectral techniques means determining the coefficients of the spectral expansion for the output quantities of interest once the spectral representations of the inputs are known. For any of these parameters, once these approximate solutions are determined, it is possible to calculate[15] Eq. (3) for the mean,

$$\mathbf{E}[\mathrm{R}] = r_0 \ , \tag{3}$$

and Eq. (4) for the standard deviation,

$$\sigma[\mathrm{R}] = \sqrt{\sum_{i=1}^{P} \langle \Psi_i, \Psi_i \rangle r_i^2} \ . \tag{4}$$

Different methodologies have been developed and applied so far for the evaluation of the output spectral coefficients, the main distinction being between intrusive and nonintrusive approaches.[15] The application of intrusive approaches requires the definition of a new mathematical problem whose solution is the set of spectral coefficients of the system unknowns. This new mathematical system is significantly larger than the original one, and it is usually solved by using a separate solver. On the other hand, nonintrusive techniques are applied by collecting a set of realizations of the original system, using the original model as a "black box." In Sec. II.A more details about the nonintrusive approach are introduced and a propagation technique based on it is presented.

II.A. Nonintrusive Spectral Projection Using Sparse Grids

Nonintrusive approaches rely on the orthogonality property of the PCE. Using this property it is possible to express the i'th coefficient of the PCE [as the one presented in Eq. (1)] by projecting the stochastic quantity of interest onto the respective polynomial. For example, the i'th coefficient of the generic stochastic quantity R is determined from the following projection:

$$r_i = \frac{\langle \mathrm{R}, \Psi_i \rangle}{\langle \Psi_i, \Psi_i \rangle} \ . \tag{5}$$

If R was, for example, an unknown or a response of the mathematical model, solving the projection integral would require the knowledge of its integrand along the integration domain. Knowing the behavior of the integrand corresponds to determining the solution of the output R at different points of the Θ space. This operation can be in principle performed by solving the problem for a finite set of realizations of the input parameters. In this way the computer code that solves the mathematical problem could be used as a black box to determine the coefficients of the PCE. Problems arise when increasing the dimension of the integral; in this case the number of realizations required in order to have a meaningful estimate for the integral becomes too large.

On the other hand, the deterministic alternative for the evaluation of the previous integral is the introduction of numerical integration techniques as quadrature formulas. In the case of a one-dimensional random problem, the numerator of Eq. (5) can be computed using the following numerical approximation:

$$\int \mathrm{R}(\xi_1) w_1(\xi_1) \, d\xi_1 = \sum_{i=1}^{nq} w_1^i \mathrm{R}(\xi_1^i) = Q_{lev}^1 \mathrm{R} \ ,$$

where ξ_1^i and w_1^i are the quadrature points and weights, respectively, associated with the one-dimensional quadrature formula employed and where nq is the number of points. This number determines the accuracy of the quadrature formula that corresponds to a level index lev, whose definition is arbitrary since its main purpose is to distinguish formulas with different orders of accuracy. In the present work we limit our analysis to Gaussian quadrature rules,[16] which can integrate with great accuracy many of the polynomial families defined by the Wiener-Askey scheme; a complete overview of univariate quadrature formulas is provided in Ref. 15. The main characteristic of Gaussian quadrature formulas is that they can integrate exactly the corresponding polynomials up to order $2nq - 1$.

For tensor product formulas the number of nodes required to build the quadrature grid is equal to nq^N, where nq is the number of quadrature points in each direction and N is the dimension of the random space. It is clear that for high-dimensional problems the method would have a computational cost comparable to or even larger than a standard Monte Carlo technique, making the approach less appealing. These requirements can be explained as a consequence of the fact that quadrature tensorization formulas are accurate for a limited set of higher-order polynomials, which are not used within the determination of the spectral coefficients. It is therefore possible to reduce the number of points of tensorization formulas by discarding this higher-order accuracy from the quadrature set. This concept led to the definition of sparse tensorization techniques for the construction of multivariate quadrature rules, known as sparse-grid techniques, first introduced by the Russian mathematician Smolyak,[17] who defined an algorithm for sparse tensor product constructions that is summarized below.

The first step for the definition of a sparse tensorization algorithm[18] is the introduction of the following difference formula:

$$\Delta_{lev}^{(1)} f \equiv (Q_{lev}^{(1)} - Q_{lev-1}^{(1)}) f$$

and

$$Q_0^{(1)} f \equiv 0 \ ,$$

where $\Delta_{lev}^{(1)} f$ is a univariate quadrature formula defined as the difference between two consecutive quadrature levels *lev*. The set of abscissas of the difference formula presented in the previous equation is defined by the union of the abscissas of the two different quadrature formulas while the weights are obtained as their difference. Because of this definition, the difference formula corresponding to the $lev + 1$ level contains all the points defined within the previous level *lev*.

After the introduction of the difference formula, the second step to implement the sparse tensorization algorithm is the introduction of the multi-index set $\mathbf{l} = (l_1, \ldots, l_N), \in \mathbb{N}^N$, whose indexes l_i are used to associate an accuracy level to each direction. Furthermore, we define the norm of this multi-index as

$$|\mathbf{l}| \equiv \sum_{i=1}^{N} l_i \ .$$

Using these definitions it is possible to write[15] the sparse-grid construction algorithm using the summation notation

$$Q_{lev}^{(N)} f \equiv \sum_{|\mathbf{l}| \le lev+N-1} (\Delta_{l_1}^{(1)} \otimes \cdots \otimes \Delta_{l_N}^{(1)}) f \ , \qquad (6)$$

according to which the final quadrature rule is built by adding a set of subgrids whose dimension *d* depends on the accuracy level used along each direction. Each subgrid $(\Delta_{l_1}^{(1)} \otimes \cdots \otimes \Delta_{l_N}^{(1)})$ corresponds to a tensorization of a set of difference formulas whose levels are defined by the value of the multi-index $\mathbf{l}$. The set of multi-indexes having norm $|\mathbf{l}| \le lev + N - 1$ (where *lev* is the accuracy level one wants to achieve for the multidimensional integral) is therefore used to generate the subgrids used in the final rule. An important consequence of this norm constraint is that the maximum dimension for an admissible subgrid is $lev - 1$, which is relatively low even when considering high-dimensional problems. This is the main aspect determining the numerical convenience of a sparse grid with respect to a tensorized one.

In general, the use of this sparse algorithm can drastically reduce the amount of quadrature points required, especially when dealing with high-dimensionality problems. Unfortunately, despite this drastic reduction, for high-dimensional problems the set of quadrature points (or, in other words, realizations) required to perform an accurate integration could still become larger than required by standard Monte Carlo approaches. The number of quadrature points generated by the sparse tensorization depends directly on the univariate formula used to build it; however, in the presence of irregular integrands and highly dimensional problems, the size of the grid would eventually become too large.[18] For this reason many authors have attempted to improve the Smolyak algorithm by introducing a way to further reduce the set of points included in the final quadrature rule.[19,20] In this paper we present an example of such improvement. Before entering into the details regarding the method, we need to introduce a few definitions useful for the implementation of sparse-grid algorithms.

II.B. Adaptive Sparse-Grid Construction Algorithms

The main idea behind the definition of an adaptive sparse-grid algorithm is that the constraint acting on the set of multi-indexes used to build the subgrids in Eq. (6) can be relaxed, therefore reducing the number of points used to generate the final quadrature formula. One of the first examples of an adaptive algorithm can be found in Ref. 18, where the authors define a sequential way to construct the multi-index set by using the reduction of the integration error as a target. Some of the subgrids included by a standard sparse-grid algorithm might introduce a negligible contribution to the final quadrature formula, depending on the stochastic direction and the quantity that is being integrated.

The reduction of the multi-index set can be performed keeping in mind that Eq. (6) represents a sum of difference formulas, which implies that a subgrid can be introduced into the final rule only if all the previous levels of the difference formula have already been included. This translates to the mathematical condition

$$\mathbf{l} - \mathbf{e}_j \in I \ , \quad \text{for } 1 \le j \le N, l_j > 1 \ , \qquad (7)$$

where

I = set of subgrids already included in the sparse grid

$\mathbf{l}$ = multi-index that corresponds to the subgrid with respect to which the admissibility is checked

$\mathbf{e}_j$ = unity vector.

According to this constraint, it is possible to build the quadrature rule starting from the subgrid defined by the first multi-index $[\mathbf{l}_1 = (1, \ldots, 1)]$ and enriching it by progressively increasing the level of the multi-index along each direction.

The idea is to find, when dealing with a high-dimensionality problem, an "optimal" quadrature formula that includes only the set of multi-indexes $\mathbf{l}_i$ causing the largest contribution to the final integral. This can be done while using a progressive multi-index approach by limiting the multi-index "enrichment" in the directions

for which the subgrid contribution to the final quantities of interest is larger than a specified tolerance. This first requires the definition of a marching algorithm to be used while sweeping through the set of multi-indexes, and second, an indicator used to determine when the contribution of a set of subgrids is below the specified tolerance.

In Refs. 18 and 19, an adaptive enrichment algorithm is proposed such that the new multi-indexes to be included within the final rule are taken from the neighborhoods of the already-included indexes. This process is performed by evaluating the contribution of each of the new multi-indexes to the final integral and by continuing the inclusion process only for the directions that cause the largest variation.

Although this algorithm can be used to integrate high-dimensional functions, it is not derived considering the application of spectral techniques as its main goal, and therefore, it does not make use of the particular aspects characterizing traditional stochastic responses. In Sec. II.C we present an alternative algorithm that can be used to implement an adaptive sparse grid when applying nonintrusive spectral techniques for uncertainty quantification.

II.C. Definition of a New Adaptive Algorithm

In this section the adaptive algorithm developed for the application of the nonintrusive spectral projection is presented. The aim of the adaptive algorithm is to successively add admissible subgrids until a desired integration tolerance is achieved. For this purpose, an indicator needs to be defined in order to determine if the contribution of an admissible subgrid is small enough for the grid to be discarded. Once this condition is met and the subgrid is dropped, the multi-index set can be updated by removing all the multi-indexes that do not satisfy the admissibility criterion. This procedure is repeated until all the subgrids of the initial set have been either included in or discarded from the final rule.

To implement the adaptive algorithm, we first define the following estimator ϵ_i for the response R, associated to the i'th subgrid:

$$\epsilon_i = \max\left[\left|\left(\frac{\delta E(\mathrm{R})}{E(\mathrm{R})}\right)\right|, \left|\left(\frac{\delta \sigma_i(\mathrm{R})}{\sigma(\mathrm{R})}\right)\right|\right] , \qquad (8)$$

where δE_i and $\delta \sigma_i$ are, respectively, the variation in the mean value and the variation in the standard deviation of the spectral expansion of R due to the i'th subgrid. If we keep in mind that each of the subgrids defined by the expansion Eq. (6) has an associated contribution ϵ_i, the aim of an adaptive algorithm would be to include in the final quadrature rule only the set of subgrids whose associated contribution is larger than a specified tolerance.

The algorithm we introduce is derived by taking into account the fact that a complex system is usually dominated by main effects and low-order interactions. This is known as the sparsity of effects principle[21] and implies that in the presence of large sets of input parameters the main influence on the stochastic response is caused by lower-order propagation components. Since a sparse grid is defined as the sum of lower-dimensional subgrids (where the maximum dimension is determined by the accuracy level *lev*), the idea of a propagation dominated by lower-order interactions is equivalent to stating that most of the contribution to the final integral will be given by lower-dimensional subgrids (e.g., one-, two-, or three-dimensional grids).

An adaptive algorithm for the construction of a sparse-grid formula has been developed taking these aspects into account. The main idea behind the algorithm is to add subgrids to the sparse grid by starting from one-dimensional grids and by progressively increasing their resolution and their size d. When the contribution ϵ_i associated with the N-dimensional grid i is smaller than a specified tolerance, the refinement process is stopped, and all the subgrids obtainable as a refinement of i are discarded from the admissible index set. In this context, the integration tolerance *tol* is the only parameter that needs to be specified.

Given the problem dimension N and a sufficiently large accuracy level (which can possibly be increased if needed), the set of multi-indexes I characterizing the complete sparse grid [defined in Eq. (6)] is generated. The aim of the algorithm is to select and evaluate from this starting set the subgrids that cause the largest contribution to the final integral. As we explained before, the subgrids present in this initial set I can be divided according to their dimension. For each subgrid this dimension, denoted as d, depends on the univariate quadrature level used in each direction and ranges from 0 to $lev - 1$.

An important aspect to address before continuing with the description of the algorithm regards the truncation of the spectral expansion used to implement the spectral projection or, in other words, the number of terms employed in the PCE. The convergence of the stochastic response R should be verified while applying the adaptive algorithm in order to have a meaningful solution. One could in principle apply the adaptive algorithm by starting from a low-order expansion and increasing the order until convergence is reached. In the presence of highly anisotropic stochastic problems, this procedure would be nonoptimal since it would require the evaluation of a PCE whose truncation depends only on the most irregular stochastic direction. A possible way to overcome this problem is the definition of an anisotropic PCE whose higher-order terms are included only for a limited set of stochastic directions.

To cover this aspect, the adaptive algorithm is initialized as follows. First, the algorithm divides all the subgrids present in I according to their dimension d and norm $|\mathbf{l}|$. The only zero-dimensional subgrid, which

corresponds to origin of the stochastic domain defined by the multi-index $\mathbf{l} = (1, \ldots, 1)$, is then evaluated. After the subgrids are divided according to their dimension and norm, the algorithm is applied in two separate steps.

First, the adaptive sparse-grid formula is enriched by adding exclusively one-dimensional grids and by using a one-dimensional PCE for each of the stochastic dimensions. This allows having an initial estimate of the convergence of the PCE along each direction, which can be used to define the order of the final spectral expansion. Second, the algorithm is continued by adding higher-dimensional subgrids, using the PCE truncation determined within the previous steps. In Secs. II.C.1 and II.C.2, these two steps are described in more detail.

II.C.1. First Step: Integration Over One-Dimensional Subgrids and Definition of a Reduced PCE

During the first part of the adaptive sparse-grid generation, the construction of the grid is performed by including quadrature points exclusively along the main axes of the stochastic domain. This is done by introducing a one-dimensional random problem for each of the stochastic random directions and by separately determining the convergence of the corresponding one-dimensional numerical quadrature.

The scope of this convergence analysis is to determine in each direction both the number of quadrature points needed to evaluate the stochastic integral and the truncation order required for the one-dimensional PCE to converge.

This corresponds to the following process repeated for each of the stochastic directions. Starting from the initial point associated to the first multi-index $\mathbf{l} = (1, \ldots, 1)$, the grid is refined by adding the smallest one-dimensional subgrid taken from the admissible multi-index set [corresponding, for example, to $\mathbf{l} = (2, \ldots, 1)$ when dealing with the first stochastic direction]. The indicator introduced in Eq. (8) is then evaluated for this grid using a first-order PCE and a second-order PCE. If, after the evaluation of this initial grid, the difference in the standard deviation obtained by using the first-order PCE and the second-order PCE is smaller than the specified tolerance, the refinement is stopped, and the PCE is assumed to be first order along the direction. If, on the contrary, the contribution of the second-order term is not negligible, the grid is refined after increasing the PCE truncation order by adding the subsequent subgrids [corresponding, for example, to $\mathbf{l} = (3, \ldots, 1)$, $\mathbf{l} = (4, \ldots, 1)$, etc.] until the indicator is smaller than the specified tolerance. A convergence test for the one-dimensional PCE is then performed, and if the spectral expansion has not converged, the previous step is repeated after the truncation order has been increased.

The outcome of this first phase is an initial collection of subgrids located along the main axes of the stochastic domain (see, for example, Fig. 1) that can be used as a starting basis for the construction of the final quadrature rule. Furthermore, the truncation orders required to achieve convergence of the one-dimensional PCEs along each direction are also known after completing this first part. We define a vector $\mathbf{p} = (p_1, \ldots, p_N)$ where each entry p_i represents the maximum order needed to represent the stochastic output when considering the corresponding variable to be the only stochastic quantity of the problem. Using this information about the convergence of the spectral expansion along each of the stochastic directions, it is possible to define a reduced multidimensional PCE by modifying the constraint on the polynomial basis introduced in Eq. (2). We introduce a new definition for the multi-index set λ [originally defined in Eq. (2)]:

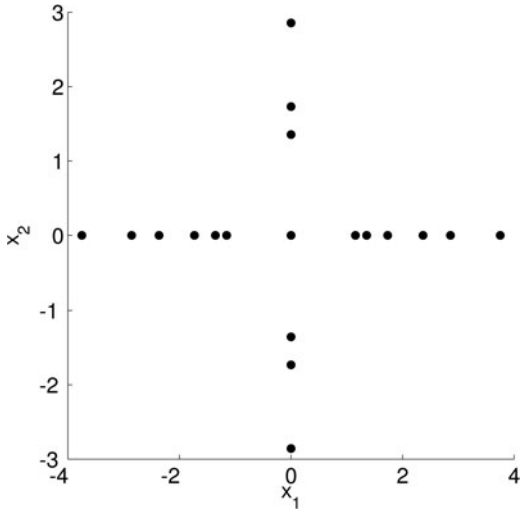

Fig. 1. Points of the quadrature formula included along the main axes at the end of the first step for a two-dimensional case.

$$\lambda(k) = \left\{ \gamma : \left(\sum_{i=1}^{N} \gamma_i = k \right) \wedge (\gamma_i \leq p_i, \text{ for } 1 \leq i \leq N) \right\}$$

$$k \leq \max(\mathbf{p}) \quad . \tag{9}$$

The definition of the new multi-index set is similar to the one presented in Eq. (2), the only difference being the constraint on the maximum polynomial order along the i'th direction. This order is now determined by the value p_i, obtained while adding the one-dimensional subgrids to the quadrature formula. Furthermore, the maximum order k used within the expansion is also determined as the maximum order needed for the convergence of the one-dimensional problems. We assume that the multi-dimensional PCE obtained by using this new constraint is converged and can be used in the following steps for the construction of the adaptive quadrature algorithm.

II.C.2. Second Step: Integration Over Higher-Dimensional Subgrids

As we explained when we first discussed the mathematical definition of sparse grid, each of the lower-dimensional subgrids used to build the final rule can be divided according to its size d and norm $|\mathbf{l}|$. When the algorithm described in Sec. II.C.1 is completed, all the one-dimensional subgrids (characterized by different norms) have been either included in or discarded from the final quadrature rule. We can therefore continue the algorithm by considering higher-dimensional subgrids. According to our algorithm, the order in which these subgrids are evaluated is first determined by their size d and then by their norm $|\mathbf{l}|$.

Figure 2 shows a scheme representing the order according to which the subgrids are evaluated. Each block in Fig. 2 represents a set of subgrids characterized by the same size and norm. The blocks in the first column represent the union of all the possible one-dimensional subgrids (which have already been evaluated within the first part of the algorithm); moving horizontally corresponds to increasing the size of the subgrids while moving vertically increases their norm (which corresponds to a higher "resolution"). After evaluating the set of one-dimensional subgrids (first column of the scheme), we proceed by analyzing the subgrids defined by the bottom block of the second column. Once the contribution of each of these two-dimensional subgrids has been calculated, we then continue by moving vertically on the scheme, therefore analyzing the two-dimensional grids associated with a higher norm. After reaching the top block of the column, we move to the third column, starting from its bottom block. This procedure is repeated until the top-right block has been evaluated.

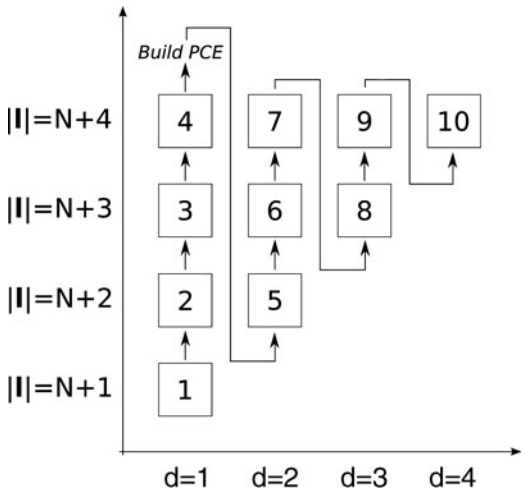

Fig. 2. Order according to which the different sets of subgrids are evaluated. Each set contains the subgrids characterized by size d and norm $|\mathbf{l}|$. N is the number of random inputs characterizing the stochastic problem.

The adaptivity within this process is implemented by enforcing, each time that a subgrid is evaluated, the condition defined in Eq. (7). This means that if the indicator Eq. (8) associated with the current subgrid is below the specified tolerance, all the subgrids that require it for their existence are discarded from the final quadrature rule. This operation introduces another condition for the algorithm to end, which is when every higher-dimensional subgrid has been discarded from the quadrature rule.

It must be kept in mind that each time a higher-dimensional subgrid is discarded from the final quadrature rule, the polynomials associated with the same multi-index must also be taken out of the PCE. This is because the grids required to evaluate the corresponding coefficients are left out of the final quadrature rule.

II.C.3. Overview of the Method

In Secs. II.C.1 and II.C.2, we introduced an algorithm that can be used to evaluate the projection coefficients of the spectral expansion in an adaptive fashion. The algorithm is based on the concept of a sparse grid and is structured in two main parts: First, the sparse quadrature points are collected along the main axes of the stochastic domain and a reduced PCE is built, and second, the integration is extended to higher-dimensional grids until a convergence for the stochastic quantities of interest is reached.

The convergence rate of this adaptive algorithm depends mainly on how many grids are discarded from the admissible multi-index set at the initial stages or, in other words, on the smoothness of the response surface of the problem. If, for example, we deal with a completely linear problem, the evaluation of two-dimensional grids would already exclude most of the multi-index set from the final quadrature rule. On the contrary, an extremely irregular output could in principle require the addition of every single grid defined by the initial set I.

The minimum requirements of the algorithm in terms of quadrature points largely depend on the number of two-dimensional subgrids added during the second phase. Assuming every single input parameter has an influence on the stochastic output of interest, this number can be expressed in the following combinatorial fashion:

$$n_{2D} = \binom{N}{2} .$$

Although the adaptive script can be used to drastically reduce the requirements associated with sparse-grid integration, increasing the number of input parameters N will eventually make the method inapplicable because of the starting set of two-dimensional grids that needs to be evaluated. This number could in principle be used as a rough criterion to estimate whether the application of the adaptive algorithm is feasible (depending on the number of random inputs N).

Depending on the regularity of the response surface, 15 to 20 parameters would therefore represent the number above which the method would be computationally more expensive than standard random sampling. This upper constraint could in theory be relaxed by finding a way to discard two-dimensional subgrids based on the evaluation of the one-dimensional ones.

In theory, the computational cost associated with spectral techniques could be further reduced by exploiting the information associated with the gradient of the stochastic response of interest with respect to the input parameters. This gradient information could be obtained by using perturbative approaches or, when dealing with functional responses, by implementing adjoint techniques such as the adjoint sensitivity analysis procedure.[1] For example, Ref. 22 presents a way to use the information associated with the gradient of a functional when dealing with nonintrusive PCE methods.

III. APPLICATION TO A MULTIPHYSICS PROBLEM

In this section we present the application of the algorithm introduced in Sec. II to an illustrative coupled time-dependent problem. The model characterizing the problem is described first, followed by the definition of the uncertainty quantification problem.

III.A. Description of the Model

The problem considered for the application of the adaptive algorithm defined in Sec. II is a coupled system that can be used to model the time-dependent behavior of a sodium fast reactor. The reference configuration used within the present analysis is the BN800, a sodium-cooled fast breeder reactor whose details have been taken from an International Atomic Energy Agency benchmark[23]; its main characteristics are summarized in Table I. The neutronics part of the coupled problem is described using a point-kinetics model[24]:

$$\frac{dQ}{dt} = \frac{\rho(t,T_f,T_c)-\beta}{\Lambda}\,Q + \sum_{k=1}^{K}\lambda_k C_k$$

and

$$\frac{dC_k}{dt} = -\lambda_k C_k + \frac{\beta_k}{\Lambda}\,Q \ ,$$

where

Q = reactor power

Λ = mean generation time

C_k = concentration of the k'th precursor group

TABLE I

Main Parameters Used for the Coupled Model

Λ (s)	4×10^{-7}
R_s (cm)	0.348
α_d (pcm/°C)	−0.68747
α_c (pcm/°C)	0.12251
δ_{clad} (cm)	0.055
v_{in} (m/s)	10
H (m)	0.91
P (MW)	2100
h_g (W/m$^2\cdot$°C)	10^4
T_{in}(°C)	355
λ_1 (1/s)	0.0124
λ_3 (1/s)	0.111
λ_4 (1/s)	0.301
λ_5 (1/s)	1.14
λ_6 (1/s)	3.01
β_1	0.00009
β_2	0.000853
β_3	0.0007
β_4	0.0014
β_5	0.0006
β_6	0.00055

β_k = delayed neutron fraction for the k'th precursor group

λ_k = decay constant for the k'th precursor group

β = total delayed-neutron fraction.

The reactivity term is considered as the sum of three different contributions:

$$\rho(t,T_f,T_c) = \rho_{ext}(t) + \delta\rho_D(T_f) + \delta\rho_C(T_c) \ .$$

The external reactivity is provided as an external input of the model while the Doppler (D) and coolant (C) reactivities represent the temperature-dependent feedback mechanisms. These reactivities are determined by spatially averaging the temperature field:

$$\delta\rho_D = \alpha_D\,\frac{1}{V_f}\iint dr\,dz\,2\pi r[\varphi_D(r,z)(T_f(r,z)-T_{rf})]$$

and

$$\delta\rho_C = \alpha_C\,\frac{1}{H}\int dz[\varphi_C(r,z)(T_c(r,z)-T_{rc})] \ ,$$

where φ_D and φ_C are the spatial weighing functions used to evaluate the integral and α_D and α_C are the first-order reactivity coefficients, modeled around a reference temperature $T_{rf,c}$. The kinetic parameters used in the point-kinetics model and the reactivity coefficients have been

obtained using the ERANOS2.2 code[25] employing the heterogeneous three-dimensional model described in Ref. 23.

To model the temperature fields required to calculate the feedbacks, the reactor domain is represented by introducing an equivalent pin geometry. In this pin the volumetric heat produced by the fission processes is transferred, across the cylindrical fuel and cladding, to the sodium coolant, which is supposed to have a fixed inlet temperature. Axial conduction along the pin is neglected, which means the heat transfer process is modeled by using a set of radial energy conservation equations. In Fig. 3 the reference geometry for the thermokinetic problem is shown. We use the following equation for the heat transfer within the fuel:

$$\rho_f c_{p,f} \frac{\partial T_f^z}{\partial t} = \frac{1}{r} \frac{\partial}{\partial r} \left(r k_f(T_f^z) \frac{\partial T_f^z}{\partial r} \right) + f^z(Q) \ ,$$

where the superscript z refers to the position along the vertical axis and $f^z(Q)$ is a shape function used to describe the distribution of the volumetric power. This function is supposed to be distributed as the fundamental neutronics solution of an equivalent homogeneous cylindrical core. Similarly, for the cladding we have

$$\rho_{cl} c_{p,cl} \frac{\partial T_{cl}^z}{\partial t} = \frac{1}{r} \frac{\partial}{\partial r} \left(r k_{cl}(T_{cl}^z) \frac{\partial T_{cl}^z}{\partial r} \right) \ .$$

The thermodynamic and heat transport properties of the fuel and the cladding have been characterized using the correlations present in Ref. 26. The boundary conditions used for the thermokinetic problem are

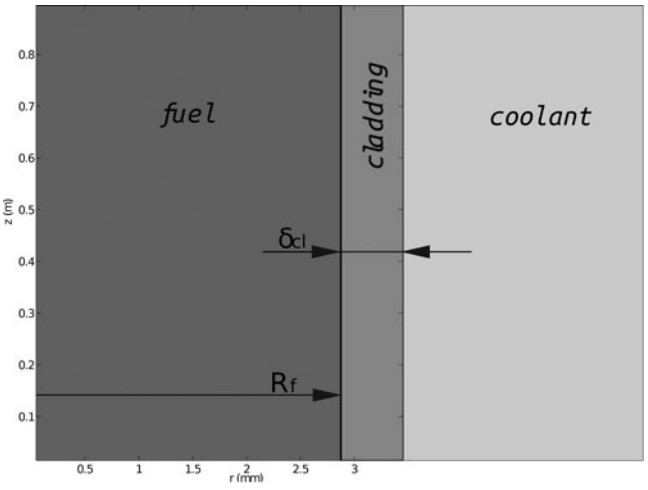

Fig. 3. Reference geometry for the thermokinetic problem.

$$\left. \frac{\partial T_f^z}{\partial r} \right|_{r=0} = 0 \ ,$$

$$k_f(T_f^z) \left. \frac{\partial T_f^z}{\partial r} \right|_{Rf} = h_g(T_{cl}^z|_{Rf+\delta_g} - T_f^z|_{Rf}) \ ,$$

$$R_f k_f(T_f^z) \left. \frac{\partial T_f^z}{\partial r} \right|_{Rf} = (R_f + \delta_g) k_{cl}(T_{cl}^z) \left. \frac{\partial T_{cl}^z}{\partial r} \right|_{Rf+\delta_g} \ ,$$

and

$$k_{cl}(T_{cl}^z) \left. \frac{\partial T_{cl}^z}{\partial r} \right|_{Rs} = h_c(T_c(z))(T_c(z) - T_{cl}^z|_{Rs}) \ ,$$

where

R_s = pin radius

R_f = radius of the fuel pellet

δ_g = size of the fuel-cladding gap

h_g = heat transfer coefficient across the gap

h_c = heat transfer coefficient of the coolant (obtained using the correlation for liquid metals introduced in Ref. 26).

The coolant temperature is determined by the following energy conservation equation, used for the equivalent channel:

$$A_c \rho c_{pc} \left[\frac{\partial T_c}{\partial t} + v_{in} \frac{\partial T_c}{\partial z} \right] - 2\pi R_s n_p h_c(T_c)(T_{cl}(R_s, z) - T_c) = 0 \ ,$$

where A_c is the equivalent flow area and n_p is the total number of fuel pins present in the reactor. A fixed coolant velocity is considered, and the boundary condition is given by a fixed coolant inlet temperature. All the parameters defined in the model are summarized in Table I.

III.B. Numerical Solution of the Model

The numerical code used to solve the coupled problem has been written by employing the CVODE time-integration modules included within the SUNDIALS suite.[27] These modules make use of a backward differential formula, which is adaptive both in terms of time stepping and order used during the time integration. The spatial discretization of the model has been performed by implementing a finite volume scheme; a linear interpolation was used to determine the surface values between volumes.

Since the conduction along the axial direction was considered to be negligible, the heat transfer problem was formulated by dividing the fuel pin into 30 axial

regions. In each of these regions, a one-dimensional radial heat conduction problem was defined and numerically solved by uniformly dividing the radial domain into 50 volumes. The boundary condition of each of these problems, given by the heat transfered between the cladding and the coolant, determined the coupling between the heat transfer equations and the energy convervation equation along the coolant channel. This equation was finally solved by dividing the channel into 150 axial volumes.

To reduce the numerical error associated with the time-integration process, the relative error used by the CVODE module was set to 10^{-7}.

III.C. Definition of an Uncertainty Quantification Problem

Based on this coupled model, we present a reference uncertainty quantification problem whose solution can be obtained by using the adaptive spectral algorithm introduced in Sec. II. This reference problem is the transient caused by the insertion of an external reactivity term ρ_{ext}. Two different types of insertion have been modeled: first, a 1 \$ step insertion and second a ramp insertion characterized by a slope of 0.75 \$/s. In both cases the external reactivity term lasts until $t_s = 1$ s and is zero afterward. Furthermore, we consider the system to be at a steady-state condition when the external reactivity is introduced at $t = 0$.

To introduce the reference uncertainty problem, some of the input parameters of the coupled model have been considered to be stochastic. A total of ten parameters were assumed to be normally distributed. They and their associated uncertainties are presented in Table II. These include the total heat transfer coefficient h_g of the gap between the fuel pellet and the cladding, the radius of the pin R_s, the thickness of the cladding δ_{clad}, the inlet velocity v_{in} and inlet temperature T_{in}, the magnitude of the external reactivity insertion ρ_{ext} (the slope for the ramp insertion), and the time at which the external reactivity is removed t_s. The fact that these parameters are normally distributed could in theory lead to nonphysical realizations of the input quantities; however, because of the relatively small uncertainties, no such realization occurred while applying the spectral and sampling approaches.

The uncertainty quantification problem arising from the presence of these stochastic input parameters has been solved first by using a standard unbiased random sampling approach using 10 000 realizations and then by applying the adaptive spectral approach defined in the first part of the paper. Because all the input parameters were normally distributed, Hermite polynomials were used to build a ten-dimensional PCE suitable to represent the stochastic quantities of the problem.

Using this set of polynomials, it is possible to spectrally represent the stochastic solutions by using the expansions

$$Q(t,\boldsymbol{\xi}) = \sum_{i=0}^{P} Q_i(t)\Psi(\boldsymbol{\xi}) \ ,$$

$$T_f(\mathbf{x},t,\boldsymbol{\xi}) = \sum_{i=0}^{P} T_{f,i}(\mathbf{x},t)\Psi(\boldsymbol{\xi}) \ ,$$

$$T_{cl}(\mathbf{x},t,\boldsymbol{\xi}) = \sum_{i=0}^{P} T_{cl,i}(\mathbf{x},t)\Psi(\boldsymbol{\xi}) \ ,$$

and

$$T_c(\mathbf{x},t,\boldsymbol{\xi}) = \sum_{i=0}^{P} T_{c,i}(\mathbf{x},t)\Psi(\boldsymbol{\xi}) \ ,$$

where $\boldsymbol{\xi}$ is a vector containing the ten independent normal variables that are used to define the stochastic parameters of Table II.

The algorithm used to implement the nonintrusive spectral method was implemented as a MATLAB script, which was used to adaptively generate the stochastic realizations corresponding to the quadrature points, run the solver, and collect the outputs of interest. The outcomes of application of the algorithm to the coupled problem just introduced are presented and discussed in Sec. IV.

IV. RESULTS: TRANSIENT CAUSED BY A STEP REACTIVITY INSERTION

In this section we analyze the response of the coupled system to a step reactivity insertion. This test problem was chosen because of the characteristic probability

TABLE II

Input Parameter (Relative) Uncertainties Used for the Definition of the Reference Problem*

Parameter	R_s	δ_{clad}	ρ_{ext}	t_s	Λ	α_d	α_c	T_{in}	h_g	v_{in}
σ	1%	1%	5%/1%	1%	1%	5%	5%	2%	10%	5%

*A 5% relative standard deviation was considered for the step insertion case while a 1% relative standard deviation was used for the ramp case.

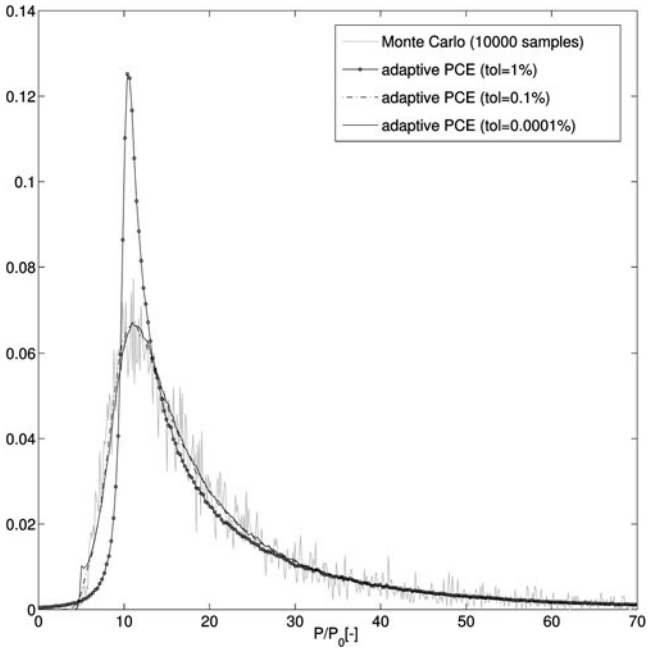

Fig. 4. Probability density function of the maximum power reached during the transient obtained by using standard Monte Carlo sampling and the adaptive algorithm with three different tolerances. These density functions were built by directly sampling the PCE of the response.

density functions associated with the presence of a large uncertainty in the magnitude of the inserted reactivity. As shown in Ref. 13, this type of transient can lead to highly skewed, non-Gaussian probability density functions of the system outputs, especially if considering the maximum power reached during the transient. For this reason, the magnitude of the external reactivity was assumed to have a 5% relative standard deviation. The values included in Table II were used for the rest of the parameters. We considered the maximum power reached during the transient as the stochastic response of interest for this stochastic problem.

Figure 4 shows the probability density function of this response obtained by using a standard unbiased sampling technique and by applying the adaptive approach using three different tolerances ($\epsilon = 1\%$, 0.1%, and 0.0001%). The skewness of these probability density functions is quite large; this means that standard perturbative approaches would have failed in the prediction of the statistical moments of interest.

Table III collects the values of the mean and of the standard deviation of the response corresponding to the different tolerances used. The number of realizations needed for the algorithm to converge is also included, together with the final PCE order employed to represent the stochastic response, as defined in Eq. (9).

The comparison between the probability density functions in Fig. 4 shows that reducing the algorithm tolerance corresponds to a convergence to the distribution obtained by using a sampling approach. The distribution built by using the largest tolerance ($\epsilon = 1\%$) is considerably different from the Monte Carlo distribution; however, this is a consequence of the fact that the algorithm convergence is verified only for the mean and for the standard deviation of the output: The values in Table III show how these values are within reasonable convergence even when using the largest tolerance. In theory one could improve this aspect by introducing higher statistical moments within the indicator defined in Eq. (8). Unfortunately, it is not possible to evaluate higher-order statistical moments by using a simple expression like the one presented in Eq. (4) for the standard deviation.

It emerges from Table III that there is clearly a value of the algorithm tolerance ($\epsilon = 0.1\%$) that represents the best compromise between the number of realizations needed and the statistical moments. When reducing this tolerance the number of points needed to converge increases considerably despite the fact that the additional stochastic information obtained is negligible.

TABLE III

Mean and Standard Deviation of the Maximum Power Reached During the Transient*

	Mean	Standard Deviation	Realizations[a]	**p**[b]
ANISP[c] ($tol = 1\%$)	21.4151	17.4932	201 (0.28)	1131111111
ANISP ($tol = 0.1\%$)	21.4169	17.5457	221 (0.31)	2141111112
ANISP ($tol = 0.0001\%$)	21.4185	17.5528	4577 (6.36)	5151231145
Monte Carlo	21.31 ± 0.17	17.43 ± 0.13	10000 (13.89)	—

*Comparison between the application of the adaptive script applied with different tolerances and Monte Carlo sampling.

[a]Number of realizations needed to evaluate the statistical moments. The corresponding CPU time, in hours, is presented between parentheses.

[b]Truncation order used along each direction of the PCE. The order of the parameters represented by **p** is the same as the order presented in Table II.

[c]ANISP: adaptive nonintrusive spectral projection.

The column including the values of **p** shows the convenience of using a truncated PCE, as defined in Eq. (9). This convenience is given by the fact that many directions can be reasonably represented by using a first-order expansion. This implies that the algorithm will converge faster since the projection integrals become easier to solve along a subset of directions. It must be pointed out that the algorithm assumes there is always a correlation between parameters, even if they are represented by using first-order expansions. One could in theory neglect some of the cross-correlation terms, for example, when dealing with two directions that are both linear, in order to further reduce the number of points required for convergence.

V. RESULTS: TRANSIENT CAUSED BY A RAMP REACTIVITY INSERTION

The adaptive sparse-grid algorithm was then applied to the transient triggered by the ramp insertion. We first analyzed a limited set of stochastic outputs. These were the maximum power and the maximum fuel, cladding, and coolant temperatures reached during the transient and the values of the same quantities at $t = 10$ s. This set of responses was used to check the convergence of the adaptive sparse-grid quadrature, with several tolerances used for this purpose.

Tables IV and V collect the outcome, in terms of standard deviation of the responses, of the application of the adaptive spectral technique. Two different tolerances have been used ($\epsilon = 1\%$ and 0.01%) corresponding to different amounts of realizations needed to reach convergence; a reference calculation obtained by using a complete sparse grid [built according to the definition introduced in Eq. (6)] was also performed. Table IV includes the standard deviations corresponding to the maximum values of the responses during the transient, while Table V presents the values of the standard deviations at $t = 10$ s. Both Tables IV and V include a column containing the output of a standard Monte Carlo sampling approach for uncertainty quantification. All the values obtained with the spectral technique are in agreement with their corresponding statistical estimators.

TABLE IV

Standard Deviations of the Maximum Values Reached During the Transient for Four Stochastic Quantities of Interest*

	$\epsilon = 10^{-2}$ $N = 201$ (0.28 h)	$\epsilon = 10^{-3}$ $N = 329$ (0.46 h)	$\epsilon = 10^{-4}$ $N = 677$ (0.94 h)	Sparse Grid $N = 12\,981$ (18 h)	Monte Carlo $N = 10\,000$ (13.88 h)
$\sigma(\max[T_f])[K]$	12.8376	12.8544	12.8632	12.8667	12.82 ± 0.08
$\sigma(T_{cl})[K]$	9.7369	9.7593	9.7597	9.7597	9.83 ± 0.06
$\sigma(T_{outlet})[K]$	12.8178	12.8165	12.8170	12.8083	12.88 ± 0.08
$\sigma(P/P_0)$	0.07578	0.07598	0.07592	0.07597	0.077 ± 0.001

*Comparison between the application of the adaptive script applied with different tolerances and Monte Carlo sampling. N is the number of realizations needed to evaluate the statistical moments, while the corresponding CPU time is presented between parentheses.

TABLE V

Standard Deviations of Four Stochastic Quantities of Interest at $t = 10$ s*

	$\epsilon = 10^{-2}$ $N = 209$ (1.16 h)	$\epsilon = 10^{-3}$ $N = 269$ (1.49 h)	$\epsilon = 10^{-4}$ $N = 713$ (3.96 h)	Sparse Grid $N = 12\,981$ (72.12 h)	Monte Carlo $N = 10\,000$ (55.55 h)
$\sigma(\max[T_f])[K]$	15.6292	15.6551	15.6840	15.6850	15.60 ± 0.1
$\sigma(T_{cl})[K]$	8.1824	8.1955	8.1955	8.1943	8.27 ± 0.06
$\sigma(T_{outlet})[K]$	11.3042	11.3248	11.3257	11.3231	11.41 ± 0.08
$\sigma(P/P_0)$	0.029871	0.029956	0.029945	0.029938	0.0302 ± 0.0004

*Comparison between the application of the adaptive script applied with different tolerances and Monte Carlo sampling. N is the number of realizations needed to evaluate the statistical moments, while the corresponding CPU time is presented between parentheses.

It is immediately noticeable how the use of different tolerances corresponds to very different numbers of realizations needed for the algorithm to converge. Using a very small tolerance corresponds to adopting the full sparse grid, or in other words, it is equivalent to including most of the subgrids defined by the initial multi-index I. The difference between the final predictions obtained is relatively small, especially considering the additional amount of computations required when using smaller tolerances. Tables IV and V show that, for the responses analyzed, using a large error ($\epsilon = 1\%$) leads to reasonable results despite the fact that the number of realizations is considerably lower if compared to the other cases. This important aspect can be explained by keeping in mind that the specified tolerance acts not only on the building process of the final sparse grid but also on the definition of the reduced PCE introduced in Eq. (9). Using a small tolerance for the convergence check of the PCE corresponds to introducing an additional set of higher-order polynomials within the final expansion. As a consequence, the projections onto this new set of polynomials will require additional quadrature points for the integration procedure to convergence. This means that if we include, because of a stronger PCE convergence criterion, higher-order polynomials that are contributing only marginally to the final spectral expansion, we will have an increase in quadrature points that is not compensated in terms of the final accuracy of our estimators. Table VI presents the order $\mathbf{p}$ [as defined in Eq. (9)] of the final PCEs used to represent the outputs at $t = 10$ s for different tolerances used within the adaptive script. Though the exact convergence of the PCE requires one to use higher-order polynomials (fourth column in Table VI), it is possible to accurately represent our stochastic outputs by using a PCE built with first- and second-order polynomials (second column). This naturally translates to a reduced number of quadrature points, as discussed in the previous paragraph.

TABLE VI

Final PCE Order $\mathbf{p}$ at $t = 10$ s Corresponding to Using Different Tolerances Within the Adaptive Algorithm

Variable	PCE Order		
	$\epsilon = 10^{-2}$	$\epsilon = 10^{-4}$	$\epsilon = 10^{-6}$
R_s	1	2	2
δ_{clad}	1	1	1
ρ_{ext}	1	1	2
t_s	1	1	1
Λ	1	1	1
α_d	2	2	2
α_c	2	2	2
T_{in}	1	1	2
h_g	2	3	3
v_{in}	1	2	2

The fact that it is possible to represent these stochastic responses with a low polynomial order also suggests that the error we would generate if we were using first-order perturbation techniques would be relatively low. If a forward perturbation approach was used (since we are dealing with many responses localized at different times and a relatively low number of parameters), we would be able to evaluate the first-order perturbation of the solution by running one nonlinear calculation and ten (corresponding to the number of input parameters) linearized ones. However, the implementation of such an approach would present two main difficulties. First, the solution of the linearized problems would need the implementation of a separate mathematical model and a dedicated numerical solver. Second, some of the perturbations introduced for this uncertainty quantification problem correspond to geometric (R_s) and time-dependent (t_s) parameters: Their modeling, though possible in theory, is not straighforward and would introduce additional errors as explained in Ref. 28.

Finally, a second test was performed on the same problem. This time every unknown of the coupled system was considered to be a stochastic response whose PCE needed to be evaluated. Figures 5 and 6 show the standard deviation of the temperature field of the system at $t = 1$ and 10 s, respectively, obtained in both cases by using a 0.1% tolerance within the adaptive algorithm. In both cases the number of realizations needed for the convergence of the complete solution was the same required for the convergence of the small subset of responses included in Table IV. This can be explained since this subset, being a set of local maxima, represents the most demanding outputs from the convergence point of view.

In both Figs. 5 and 6, a very large standard deviation is present close to the fuel-cladding gap; this is expected since its heat transfer coefficient presents a large uncertainty (10%). It is also interesting to see how, while at the beginning of the transient the uncertainty profile is rather symmetrical with respect to the axial direction, after 10 s the uncertainty tends to be larger along the axial direction, probably due to the uncertainties associated with the coolant inlet temperature and velocity.

Finally, a remarkable feature of spectral methods is that, once the spectral solution is known, it is possible to have a breakdown of the stochastic effects arising from each of the stochastic inputs. This is because our solution is now expressed as a function of the input parameters, which makes it easy to perform sensitivity analysis. Evaluating the coefficients of the PCE Eq. (1) corresponds to determining the dependency of the stochastic outputs of interest with respect to the input random variables $\boldsymbol{\xi}$ used to model the random inputs. Once these coefficients are known, we can estimate the effects of

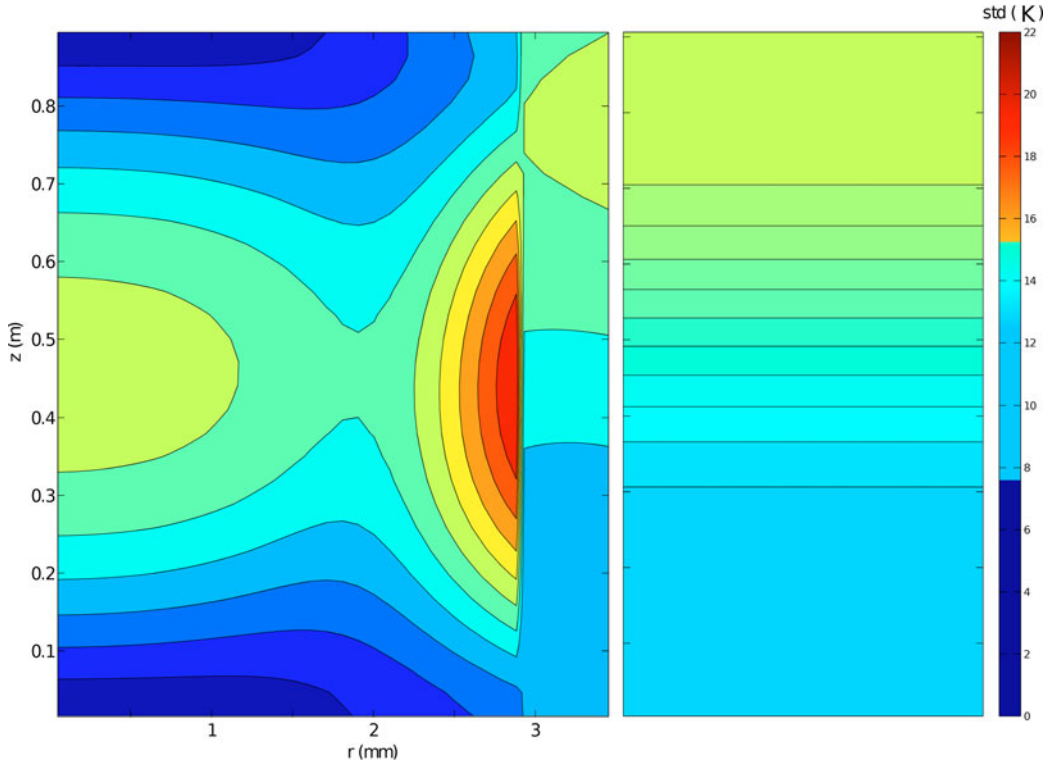

Fig. 5. Standard deviation of the system temperature field at $t = 1$ s, obtained by using $\epsilon = 0.1\%$; 329 realizations were needed to reach convergence.

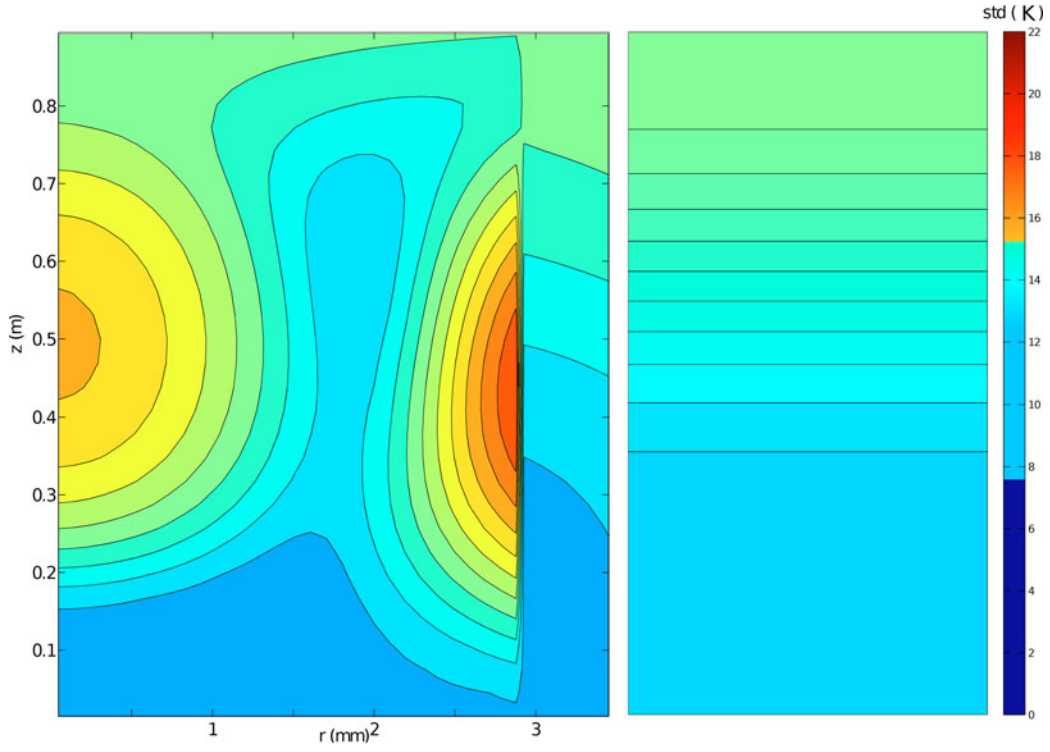

Fig. 6. Standard deviation of the system temperature field at $t = 10$ s, obtained by using $\epsilon = 0.1\%$; 269 realizations were needed to reach convergence.

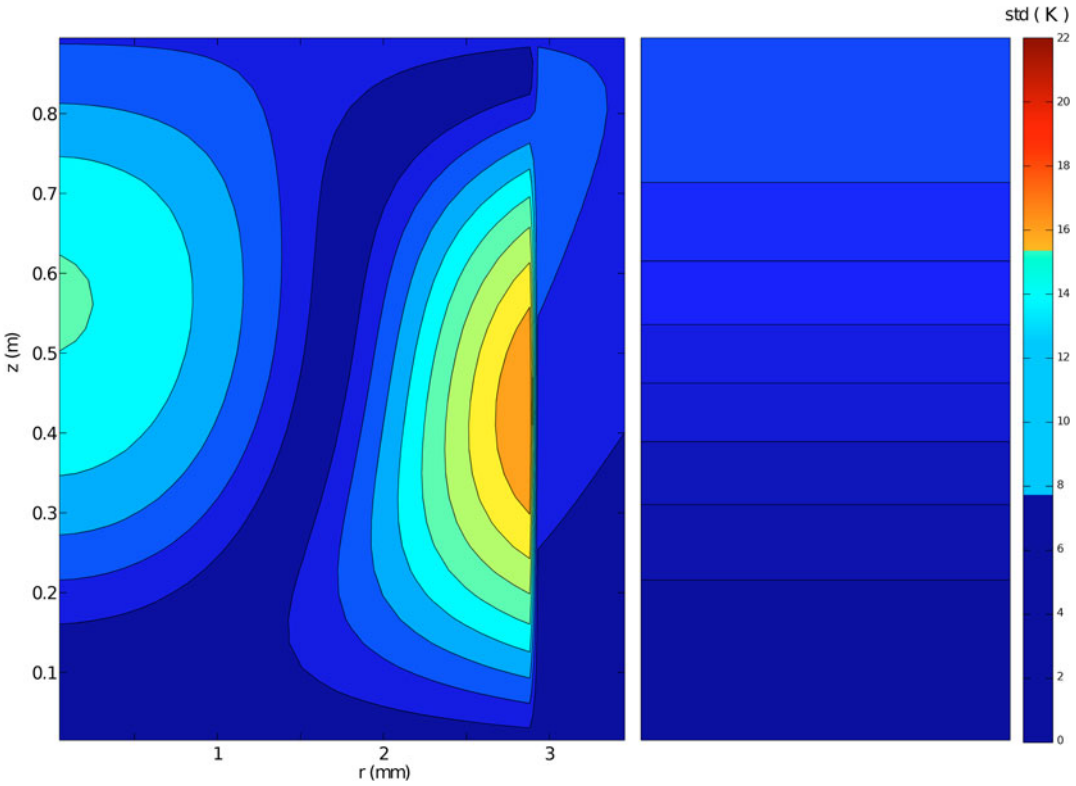

Fig. 7. Standard deviation of the temperature field at $t = 10$ s obtained by considering the heat transfer coefficient of the gap as the only stochastic variable of the PCE.

any single input parameter by considering the corresponding random variable ξ_i as the only nonzero term within the expansion Eq. (1).

For example, Fig. 7 shows the influence on the solution at $t = 10$ s of the uncertainty introduced by the heat transfer coefficient of the gap. It is possible to appreciate from Fig. 7 the presence of a peak in the proximity of the gap, which is responsible for the large standard deviation shown in Fig. 6.

VI. CONCLUSIONS

In this paper we introduced a new algorithm for the implementation of an adaptive quadrature rule, based on the notion of a sparse grid. The technique is based on the sequential construction of a sparse grid by the addition of lower-dimensional subgrids, which are progressively increased in resolution and dimension. The construction process is divided into two main steps. First, the algorithm adds quadrature points exclusively along the main axes of the stochastic domain. During this phase the convergence of the PCE is assessed and a reduced multidimensional PCE is defined. This reduced PCE is then used within the second part of the algorithm, which focuses on the addition of higher-dimensional subgrids to the final quadrature rule. The main approximation introduced by this algorithm is that higher-dimensional grids are not included in the final rule if obtained as the tensorization of lower-dimensional grids associated with a negligible contribution.

The adaptive sparse-grid algorithm has been tested for a reference stochastic case defined using a coupled problem. The results obtained by applying the algorithm show that by using the right integration tolerance it is possible to obtain the stochastic information of the system with a reduced number of quadrature points. When using very small tolerances, the final quadrature set built by the adaptive algorithm converges to a standard sparse-grid rule; however, by relaxing this constraint it is possible to achieve a considerable reduction of the quadrature points preserving the statistical moments of the outputs of interest.

The only requirement of the method is the collection of a limited set of realizations of the stochastic outputs; its implementation is therefore relatively easy. Furthermore, the information associated to the final outputs allows one not only to evaluate the statistical moments of interest but also to perform sensitivity analysis of the problem.

Our future work will focus on the application of the method to larger systems, in terms of number of input

variables. The main limitation of the method is given by the number of two-dimensional subgrids that need to be included in the final quadrature rule. The definition of a criterion to select these two-dimensional subgrids before the actual evaluation would therefore be needed to further reduce the computational requirements associated with the technique.

REFERENCES

1. D. G. CACUCI, *Sensitivity and Uncertainty Analysis, Volume 1: Theory*, Chapman and Hall CRC (2003).

2. N. WIENER, "The Homogeneous Chaos," *Am. J. Math.*, **60**, 897 (1938).

3. R. G. GHANEM and P. D. SPANOS, *Stochastic Finite Elements: A Spectral Approach*, Dover Publications (1991).

4. H. N. NAJM, "Uncertainty Quantification and Polynomial Chaos Techniques in Computational Fluid Dynamics," *Annu. Rev. Fluid Mech.*, **41**, 35 (2009).

5. L. MATHELIN, M. Y. HUSSAINI, and T. A. ZANG, "Stochastic Approaches to Uncertainty Quantification in CFD Simulations," *Numer. Algorithms*, **38**, 209 (2005).

6. R. G. GHANEM and P. D. SPANOS, "Spectral Techniques for Stochastic Finite Elements," *Arch. Comput. Meth. Eng.*, **4**, 63 (1997).

7. M. M. R. WILLIAMS, "Polynomial Chaos Functions and Neutron Diffusion," *Nucl. Sci. Eng.*, **155**, 109 (2007).

8. M. M. R. WILLIAMS, "Polynomial Chaos Functions and Stochastic Differential Equations," *Ann. Nucl. Energy*, **33**, 774 (2006).

9. M. D. EATON and M. M. R. WILLIAMS, "A Probabilistic Study of the Influence of Parameter Uncertainty on Solutions of the Neutron Transport Equation," *Prog. Nucl. Energy*, **52**, 580 (2010).

10. E. D. FICHTL, "Stochastic Methods for Uncertainty Quantification in Radiation Transport," PhD Thesis, University of New Mexico (2009).

11. O. RODERICK, M. ANITESCU, and P. FISCHER, "Polynomial Regression Approaches Using Derivative Information for Uncertainty Quantification," *Nucl. Sci. Eng.*, **164**, 122 (2010).

12. A. W. HAGUES, M. M. R. WILLIAMS, and M. D. EATON, "A Probabilistic Study of the Effect of Retardation Factor Uncertainty Using a Compartment Model for Radionuclide Release into the Biosphere," *Ann. Nucl. Energy*, **37**, 1197 (2010).

13. L. GILLI et al., "Performing Uncertainty Analysis of a Nonlinear Point-Kinetics/Lumped Parameters Problem Using Polynomial Chaos Techniques," *Ann. Nucl. Energy*, **40**, *1*, 35 (2012).

14. D. XIU and G. E. KARNIADAKIS, "The Wiener-Askey Polynomial Chaos for Stochastic Differential Equations," *SIAM J. Sci. Comput.*, **24**, 619 (2002).

15. O. P. LE MAITRE and O. M. KNIO, *Spectral Methods for Uncertainty Quantification*, Springer (2010).

16. M. ABRAMOWITZ and I. A. STEGUN, *Handbook of Mathematical Functions*, Dover, New York (1964).

17. S. SMOLYAK, "Quadrature and Interpolation Formulas for Tensor Products of Certain Classes of Functions," *Dokl. Akad. Nauk SSSR*, **4**, 240 (1963).

18. T. GERSTNER and M. GRIEBEL, "Numerical Integration Using Sparse Grids," *Numer. Algorithms*, **18**, 209 (1998).

19. T. GERSTNER and M. GRIEBEL, "Dimension-Adaptive Tensor-Product Quadrature," *Computing*, **71**, *1*, 65 (2003).

20. BA. GANAPATHYSUBRAMANIAN and N. ZABARAS, "Sparse Grid Collocation Schemes for Stochastic Natural Convection Problems," *J. Comput. Phys.*, **225**, *1*, 652 (2007).

21. C. F. J. WU and M. HAMADA, *Experiments: Planning, Analysis, and Parameter Design Optimization*, John Wiley and Sons (2000).

22. A. K. ALEKSEEV, I. M. NAVON, and M. E. ZELENTSOV, "The Estimation of Functional Uncertainty Using Polynomial Chaos and Adjoint Equations," *Int. J. Numer. Methods Fluids*, **67**, *3*, 328 (2011).

23. "Evaluation of Benchmark Calculations on a Fast Power Reactor Core with Near Zero Sodium Void Effect," IAEA-TECDOC731, International Atomic Energy Agency (1994).

24. J. J. DUDERSTADT and L. J. HAMILTON, *Nuclear Reactor Analysis*, John Wiley and Sons (1976).

25. G. RIMPAULT et al., "The ERANOS Code and Data System for Fast Reactor Neutronic Analyses," *Proc. PHYSOR 2002*, Seoul, Korea, October 7–10, 2002, American Nuclear Society (2002).

26. A. E. WALTAR, D. R. TODD, and P. V. TSVETKOV, *Fast Spectrum Reactors*, Springer (2012).

27. A. C. HINDMARSH et al., "SUNDIALS: Suite of Nonlinear and Differential/Algebraic Equation Solvers," *ACM Trans. Math. Software*, **31**, *3*, 363 (2005).

28. J. A. FAVORITE and K. C. BLEDSOE, "Eigenvalue Sensitivity to System Dimensions," *Ann. Nucl. Energy*, **37**, *4*, 522 (2010).